polymers

MDPI

Article

Nanocelluloses reinforced bio-waterborne polyurethane

M. E. Victoria Hormaiztegui [1,2], Diana Marin [1] , Piedad Gañán [3] , Pablo Stefani [1], Verónica Mucci [1] and Mirta I. Aranguren [1,*]

[1] Instituto de Investigaciones en Ciencia y Tecnología de Materiales (INTEMA), UNMDP, CONICET, Facultad de Ingeniería, Av. Juan B Justo 4302, (7600) Mar del Plata, Argentina.; marangur@fi.mdp.edu.ar, pmstefan@fi.mdp.edu.ar, vmucci@fi.mdp.edu.ar

[2] Present address: Centro de Investigación y Desarrollo en Ciencia y Tecnología de Materiales (CITEMA), Universidad Tecnológica Nacional (UTN) - Comisión de Investigaciones Científicas de la Provincia de Buenos Aires (CIC), Facultad Regional La Plata, Av. 60 y 124, (1923) Berisso, Buenos Aires, Argentina; mevhormaiztegui@frlp.utn.edu.ar

[3] Facultad de Ingeniería Química, Universidad Pontificia Bolivariana (UPB). Circular 1, No 70-01 Medellín, Colombia; piedad.ganan@upb.edu.co

* Correspondence: marangur@fi.mdp.edu.ar

Abstract: The aim of this work was to evaluate the influence of two kinds of bio- nano-reinforcements, cellulose nanocrystals (CNC) and bacterial cellulose (BC), on the properties of castor oil-based waterborne polyurethane (WBPU) films. CNC were obtained by acidolysis of microcrystalline cellulose, while BC was produced from *Komagataeibacter medellinensis*. WBPU/BC composite was prepared by impregnation of a BC membrane and further drying, while WBPU/CNC composite was obtained by casting. The nanoreinforcement was adequately dispersed in the polymer using any of the preparation methods, obtaining optically transparent compounds. Thermal gravimetric analysis, Fourier-transform infrared spectroscopy, field emission scanning electron microscopy, dynamical mechanical analysis, differential scanning calorimetry, contact angle and water absorption tests were carried out to analyze the chemical, physical and thermal properties as well as the morphology of nanocelluloses and composites. The incorporation of nanoreinforcements into the formulation increased the storage modulus above the glass transition temperature of the polymer. The thermal stability of the BC-reinforced composites was slightly higher than that CNC composites. In addition, BC allowed to maintain the structural integrity of the composites films when they were immersed in water. The results were related to the relatively high thermal stability and the particular three-dimensional interconnected reticular morphology of BC.

Keywords: bio-based waterborne polyurethane, castor oil, bacterial cellulose, cellulose nanocrystals

Citation: Lastname, F.; Lastname, F.; Lastname, F. Title. *Polymers* **2021**, *13*, x. https://doi.org/10.3390/xxxxx

Academic Editor: Firstname Lastname

Received: date
Accepted: date
Published: date

1. Introduction

The continuous growing global interest in reducing the environmental pollution has triggered and sustained the research and development of environmentally friendly polymeric materials to replace polymers of synthetic origin in different applications [1,2].

In particular, polyurethanes (PUs) have received much attention. They are versatile polymers that find applications in various fields in the form of elastomers, foams, matrices of structural composites, fibers, adhesives, coatings, etc. Since PUs are soluble in organic chemicals, their traditional use as coatings and their preparation as thin self-standing films is associated with the release of volatile organic compounds (VOCs) into the atmosphere. Therefore, important efforts have been devoted to reduce this problem and thus, during the last few decades, there has been a growing preference towards the use of waterborne polyurethanes (WBPU) that consist in stable suspensions of PU nanodroplets in water [3]. With the introduction of biobased polyols in the market, the preparation of

biobased WBPU has also progressed with the aim of producing greener alternatives to traditional materials.

The synthesis of WBPU requires the incorporation of an emulsifier that allows the stabilization of the PU aqueous dispersion. Frequently, this is achieved by using as co-monomer a short diol containing an ionizable group in it molecular structure. Anionic and cationic WBPU can be prepared, although the former are more common. In the case of an anionic WBPU, the internal emulsifier is a diol containing also a carboxyl group, while a counterion must be incorporated in the aqueous solution media [4,5]. Bio-WBPU are also prepared with this technique and vegetable oils have shown to be a particularly attractive source for the preparation of polyols. These polyols are obtained *via* the chemical modification of the oil, or from the preparation of monomers from which the polyols are synthesized [6–8]. In few cases, the vegetable oil can be used directly as a polyol, which is the case of castor oil that has hydroxyl groups in the esterified ricinoleic acid chains [6].

In order to improve or tailor properties to meet specific requirements, polyurethane aqueous dispersions have also been modified by the addition of different nanoparticles inorganic or biobased ones, to produce self-standing films or coating formulations [3,9–13]. Transparent films, mostly from anionic WBPU, have been produced from castor oil and castor oil derived monomers, also containing different nanofillers/reinforcements (cellulose nanocrystals [14–16], nanosilica [10,17], nanosilver [18] and nanoclays [19]).

One of the most studied bioreinforcements is cellulose, because of its worldwide availability, outstanding properties and low cost [20–22]. Additionally to these benefits, micro and nanocelluloses can be handled in aqueous suspension and thus easily incorporated in the bio-WBPU formulation [16,23].

When cellulose is obtained from plants, it must be separated from the other components present in the raw materials. This *top-down* process consists in the disintegration of the vegetable biomass, followed by purification of the cellulose and then, usually a combination of mechanical and chemical (or enzymatic) steps that lead to the defibrillation of the cellulose microfibers, to obtain fibrils of a few nanometers in thickness. When the final product is cellulose nanocrystals (CNC), the process continues with the acidolysis of the fibrils (a strong acid such as sulfuric acid is frequently used) that degrades preferentially the amorphous regions and allows to end up with acicular nanoparticles, CNC, with thickness usually in the range of 5-10 nm and lengths of 150-200 nm [20,22,24,25].

Some researchers have investigated the use of CNC as reinforcement of PU and WBPU, taking advantage of the interfacial interaction developed between the materials through H-bonds. It has been reported that cellulose-PU interactions have effects on phase separation of segmented PU and on the crystallization of some of these polymers [15,26,27].

On the other hand, bacterial nanocellulose (BC) is obtained *via* a *bottom-up* process, which consists of the external secretion of different bacteria, like *Acetobacter* and *Glucanobacter*, which produce a nanofibrillar 3D-entangled pellicle a protective measure. The nanofibrils (thickness of 2-4 nm) are extruded through specific points in the bacterial cell wall and aggregate to form long ribbons of high crystallinity, but also with amorphous segments that make them very flexible [28,29].

After the BC pellicles are carefully washed to remove any impurity, they can be used in their hydrated state or as freeze dried membranes [30]. Besides, in some cases, they have been used as a source in the production of nanocrystals [31]. As in the case of the CNC, BC can also be used as reinforcement of WBPU.

Comparatively, a lower number of works have been produced that address the preparation of WBPU with BC nanocomposites. Urbina et al. (2019) prepared such a composite by immersion of a BC wet membrane into a commercial synthetic WBPU [32]. The composite showed shape memory behavior and was activated by immersion in water at 40 °C. The authors found a much enhanced recovery because of the incorporation of BC. Feng et al. (2020) also prepared a WBPU composite with BC using a commercial synthetic polymer to prepare a nasal stent [33].

In this work, two very different types of nanocelluloses (BC and CNC) were used in the preparation of reinforced films based on a waterborne polyurethane based on castor oil as the only polyol source. Self-standing films are discussed in this work, which could be used as protective films. In the particular case of CNC, the suspension could also be used as coatings of metals and woods as it has been previously reported [34].

2. Materials and Methods

2.1. Raw materials

Castor oil (CO, Parafarm®, OH number=177.21 mg/mg of CO, f=2.9) and dimethylolpropionic acid (DMPA, Sigma-Aldrich Corp., 98 % purity, f=2) were dried under vacuum before use it. Isophorone diisocyanate (IPDI, 98 % purity, NCO number = 24.06 % determined by ASTM D2572, f=2), dibutyltin dilaurate (DBTDL, 95 % purity), triethylamine (TEA, 99 % purity), acetone and dimethylformamide (DMF) were purchased from Sigma-Aldrich Corp. and used without purification.

In order to obtain cellulose nanocrystals (CNC), microcrystalline cellulose powder (MCC) purchased from Sigma–Aldrich Corp. was used. Sulfuric acid (98% w/v, Anedra) was used to proceed with the cellulose acid hydrolysis. Bi-distilled water and Spectra/Por Standard RC dialysis tubing were used in the dialysis of the cellulose crystals suspension. Citric acid (Biopack), glucose (Britania), peptone (Britania), Sodium phosphate dibasic anhydro (Na_2HPO_4, Cicarelli), potassium hydroxide (KOH, Merck) were used to obtain bacterial cellulose.

2.2. Synthesis of WBPU

Castor oil and DMPA (OH equivalent molar ratio of CO to DMPA= 1.0) were fed into a five necked glass reactor with N_2 inlet to reduce any contribution from ambient humidity. Then, IPDI (NCO/OH ratio = 1.4) and DBTDL (1 wt.% with respect to the total reaction mass) were added and the reaction was allowed to proceed under mixing at 78 °C for 5 h [4,35]. Acetone was added to avoid a too rapid increase of the viscosity. Then, after allowing the temperature to drop to 60 °C, TEA (in equivalent ratio with respect to the acid groups of the DMPA) was added, followed by 0.5 h stirring. Finally, the mixture was vigorously stirred (800 rpm) for 0.5 h, while distilled water (100 mL) was added into the reactor to produce the polyurethane dispersion. The final dispersion was fed into a rotary evaporator to eliminate the remaining acetone (at 30 °C). The waterborne polyurethane was coded WBPU.

2.3. Synthesis of Nanocelluloses

The bacterial cellulose (BC) was obtained from *Komagataeibacter medellinensis* (previously named as *Gluconobacter medellinensis sp.nov.*), isolated from vinegar [36,37]. The bacteria were grown in commercial H&S medium (2 wt./vol.% of glucose, 0.5 wt./vol.% of peptone, 0.5 wt./vol.% of yeast and 0.27 wt./vol. % of Na_2HPO_4 and 1.15 g/L of citric acid, at pH=3.5). Incubation was carried out for one week at 28 °C, in an incubator oven. The films were removed from the medium and to remove residues from the culture medium, they were treated with 5 wt.% potassium hydroxide for 12 h at room temperature. Finally, the BC films were washed with distilled water until reaching a neutral pH.

It should be noticed that the strain used here produces a large amount of cellulose at low pH (3.5), indicating that it exhibits high tolerance to acidic environments while optimally producing BC. This is highly desirable in industrial fermentation processes, because microbial contamination can also avoided, since most microorganisms are unable to grow at low pH [37].

The CNC were synthetized using acid hydrolysis of MCC, according to a previously reported technique used in our laboratory [38]. MCC was added in distilled water and dispersed by mechanical stirring until the suspension was homogenized. Then,

concentrated sulfuric acid was slowly added keeping the temperature below 20 °C with an ice bath. After that, the temperature was set to 44 °C and the suspension was mixed with vigorous stirring for 2 h. Afterwards, the suspension was diluted with distilled water (1:4) and then, dialyzed against distilled water and bidistilled water until the water pH was reached. A polyester cloth with pore size of 18 μm was used in order to filter the CNC suspension and separate potential remaining unreacted MCC.

2.4. Composites preparation

Neat WBPU film was prepared by casting (30 °C overnight). In the case of composite films, two different paths were followed.

Impregnation of a wet BC membrane by the WBPU dispersion was carried out to prepare the composite. The WBPU dispersion was added to the BC membrane placed in a glass Petri dish coated with non-stick adhesive paper. Impregnation was carried out for a full day at room temperature, followed by drying the film in a convection oven at 30 °C overnight. A concentration of 1.35 wt.% of BC was achieved with this method.

CNC composite film was prepared by mixing the two aqueous suspensions, the matrix (WBPU) and the reinforcement, with mechanical stirring for 30 min (750 rpm) and bath sonication for 5 min (37 Hz, 100% power, 5 min). Casting of the mixed dispersion in glass Petri dish coated with non-stick adhesive paper at 30 °C overnight was performed to achive a concentration of 1.0 wt.% CNC (dry base). Figure 1 shows a simple scheme of both preparation processes.

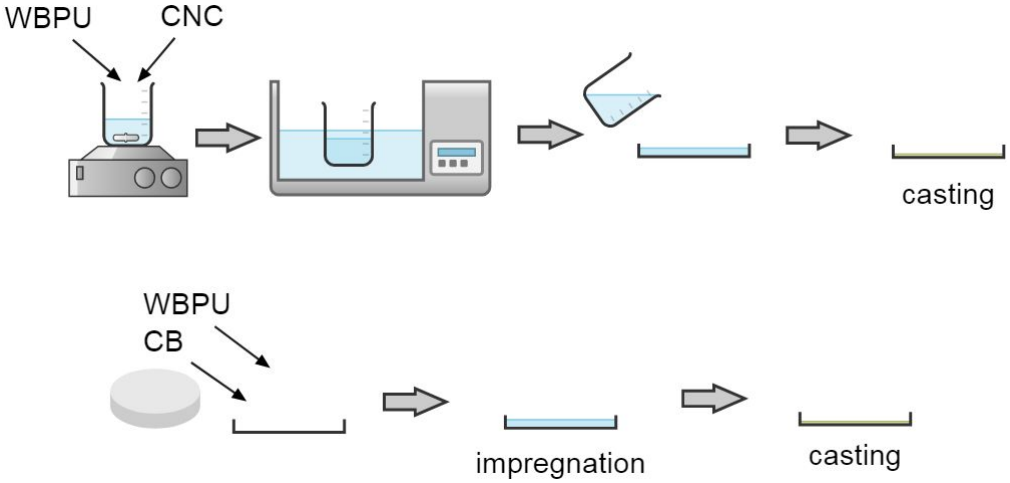

Figure 1. Preparation of the films containing WBPU and CNC or BC.

2.5. Characterization methods

A Bruker IFS 25 spectrometer at ambient temperature, with an attenuated total reflectance (ATR) unit, was used to obtain FTIR spectra of WBPU. The infrared spectra were recorded at 64 scans with a resolution of 4 cm^{-1}. The composite films were also characterized with this technique.

To determine the crystallinity of the cellulose and the influence as reinforcement in the composites of WBPU, an X ray diffractometer (X PANalytical X' Pert PRO, with Cu (Kα) radiation, wavelength: 1.54187 Å). Samples were scanned from 2θ = 5 to 60°, at a scanning speed of 0.016° s^{-1}.

A differential scanning calorimeter equipment (DSC Pyris 1 Perkin Elmer, with an electric intracooler as refrigerator unit) was used in order to obtain DSC thermograms of WBPU and its composites. Samples were scanned from -70 °C to 200 °C, at 10 °C min^{-1} under N_2 atmosphere.

The thermal stability of WBPU and its composites was characterized using a TGA-50 Shimadzu. Samples were heated up from room temperature to 500 °C at a heating rate of 10 °C min^{-1} under N_2 atmosphere.

A rheometer (Anton Paar Physica MCR 301) was used to determine the viscoelastic properties of the samples, by dynamic torsion of solid rectangle bars in the range of linear viscoelastic behavior. Samples were test from -80 °C to 140 °C, at a scanning rate of 5 °C min^{-1} with a constant strain of 0.05 % and a frequency of 1 Hz.

The observations of the freeze dried BC membrane and the cross section surfaces of the films after cryogenic fracture were carried out using a scanning electron microscope (SEM) Jeol JM-6460LV, with a voltage of 15 kV. The samples were previously placed in a sample holder and coated with gold and platinum. CNC morphology was examined by field emission scanning electron microscopy (FE-SEM) using a Zeiss-Supra 40 microscope, with accelerating voltage of 5 kV. The CNC dispersion was diluted at 0.001 % and sonicated for 30 minutes; then a drop was put onto the holder to dry, followed by coating with a layer of gold.

A goniometer OCA 15LHT Plus photo-microscope Dataphysics was used to measure the static contact angle of composites and neat WBPU films, using di-iodomethane (Sigma-Aldrich Corp.) and bidistilled water at room temperature. Using a micropipette, a drop of 5 μl of each liquid was deposited on the surface of the samples. After 30 s (time to damp the drop oscillation) a photograph was taken using a high-resolution camera. A Microsoft Photoeditor Software was used to measure the angle between the coating surface and the tangent line to the drop of liquid.

In order to register changes in the films, due to degradation/dissolution in water, the different samples were immersed in double-distilled water. Photographs were taken before immersion and after a specified test time. The sample was recovered from the water using tweezers and its surface was dried before the "after" picture was taken.

3. Results and discussion

3.1. Characterization of nanocelluloses

3.1.1. Microscopic structure of the nanocelluloses

Figure 2.a show the typical gel-like appearance of a BC membrane and Figure 2.b shows the three-dimensional interconnected reticular pellicle formed by the nanosize ribbon-like fibers. The ribbons within the network are uniformly distributed and randomly oriented, probably because the microorganism duplicates the sites for cellulose synthesis before division, and therefore the mother and the daughters cells present the same amount of active sites for synthesizing ribbons of constant dimensions. In this process, there is no break of the cellulose ribbon after splitting, only the creation of branch points [39,40].

Figures 2.c and d show digital and FE-SEM images of the CNC produced by sulfuric acidolysis of the microcrystalline cellulose. The FE-SEM image allows to better observe the thin structure of the crystals, the size distribution is quite narrow and there are no traces of micrometer sized fibers.

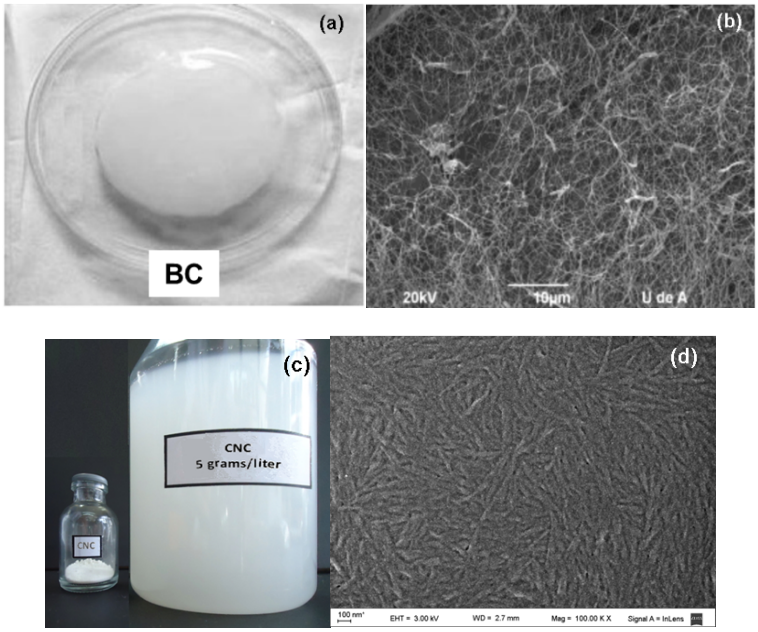

Figure 2. (a) Digital image of the wet BC membrane; **(b)** SEM image of the same sample after being lyophilized; **(c)** digital image of CNC powder and water dispersion; **(d)** FE-SEM image of CNC.

3.1.2. FTIR characterization

Figure 3.a shows the IR spectra of the two nanocelluloses used in the study. The characteristic peaks of cellulose type I are present in these spectra [41]. At 1429 cm^{-1} appears the peak corresponding to the symmetric bending of CH2, [42] at 1105 cm−1 the stretch of the C-O-C bond and at 895 cm^{-1} appears the band due to the glycosidic β-linkage of cellulose [43–52].

Comparison of the two spectra shows that the bands in the 1500-895 cm^{-1} region are of relative lower intensity in the CNC spectrum. According to previous publications [53], this suggests that the CNC is less crystalline that BC, difference that will be further considered in the analysis of the X ray diffraction characterization.

There are also differences in the absorption band of the OH groups (3650-3120 cm^{-1}), which are related to differences in the H-bonding present in the two nanocelluloses, with the free OH appearing at higher wavenumbers.

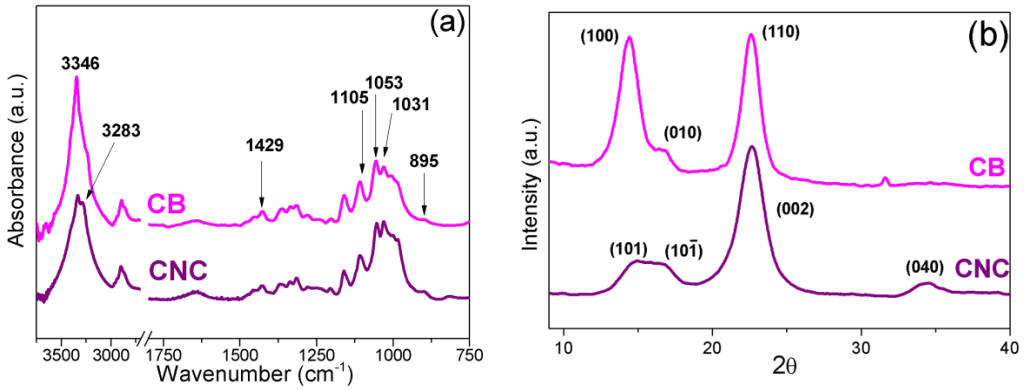

Figure 3. (a) FTIR spectra of the two nanocelluloses: BC and CNC; **(b)** X ray spectra of BC and CNC

3.1.3. X ray characterization

The X ray diffractograms of the two nanocelluloses are shown in Figure 3.b. Although both spectra show that the samples correspond to cellulose type I, the hydrogen bonding

between and within cellulose molecules are different in the two celluloses used. Thus, bacterial cellulose is rich in cellulose type I_α, while CNC shows the typical spectrum of cellulose type I_β [54,55].

The peaks in the BC spectrum are assigned to the crystallographic planes (100), (010) y (110), corresponding to the 2θ = 14.4°, 16.7° and 22.6° [36]. The high intensity of the peak corresponding to plane 100 is due to the strong monoplanar structure of the fibers of BC that have ribbon like structure and are preferentially oriented parallel to the surface of the film during drying [36,39,56]. This feature is characteristic of BC, although the relative height of the peaks varies with the substrate of the culture [57,58].

On the other hand, the X ray spectrum of the CNC shows the peaks corresponding to the planes (101), ($10\bar{1}$), (002) appearing at 2θ = 14.8°, 16.7° and 22.6°. In this case, as it is typical from cellulose of high order plants, the peak with the highest intensity corresponds to the plane (002).

The calculation of the degree of crystallinity by a deconvolution method [59–61] lead to the result that is the BC is more crystalline that the CNC, 80.79 and 71.43 %, respectively. The result is in agreement with the observation of the FTIR spectra as already discussed.

3.1.4. Thermal degradation (Thermo-gravimetric analysis, TGA)

Figure 4 shows the TG and derivative signal resulting from the thermal degradation under N_2 atmosphere of the two celluloses and after an initial loss of water. While the main degradation of BC occurs between 300-400 °C (Figure 4.a) with the maximum peak at 375 °C (Figure 4.b), in agreement with cellulose degradation profile [62–64], the main degradation of CNC occurs in the range of 230-300 °C (Figure 4.a) with a peak at ~281 °C (Figure 4.b). This low temperature degradation is the result of the obtaining method, which leaves sulfate groups on the surface and reduces the thermal stability of the CNC, also a minor degradation step centered about 350 °C appear. Furthermore, due to the presence of sulfate groups in the CNC sample, the final char is higher for this sample than for the BC one (24 and 13 %, respectively, at 650 °C) [31,65,66].

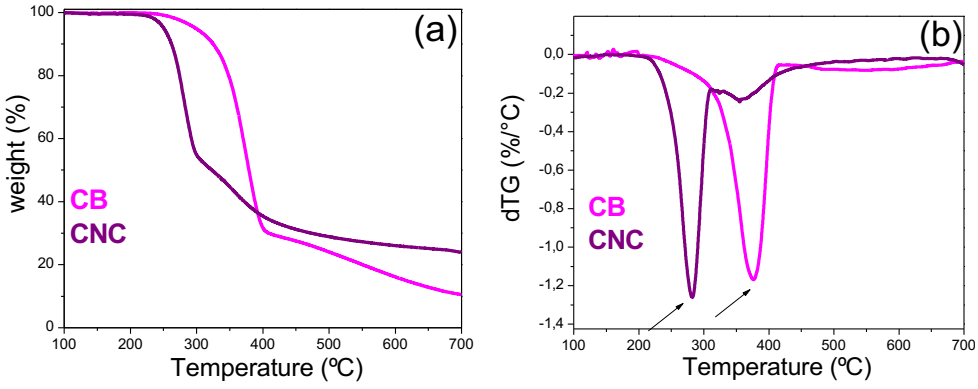

Figure 4. (a) Thermal degradation curves (TG); **(b)** derivative signal (dTG) obtained under N_2 atmosphere for BC and CNC.

Roman and Winter [31], found that even a small concentration of sulfate groups on the surface of nanocrystals obtained from BC, is enough to produce a large reduction of the degradation temperature of the nanoparticles. Elimination of the sulfate groups requires relatively low energy and facilitates the depolymerization of the cellulose, beginning with the chains close to these groups [63,67]. The second minor peak that appears in the degradation of CNC is due to the decomposition of the solid remains from the previous step. The sulfate groups are also responsible of the higher char in the CNC sample and it has been reported that they also have a flame retardant effect [31]. Our results are in agreement with those observations.

3.2. Characterization of the composite films

3.2.1.Optical aspect and SEM topology

Figure 5.a shows images of the neat WBPU and the nanocomposite films. In the image of the neat WBPU film, it can be seen that it has copied the texture of the Teflon film used as base in the Petri dish. All films were optically transparent, at least in the range of thickness used in the study (600-650 μm).

The SEM images (Figure 5.b) show that low temperature fracture resulted in a brittle fracture with mirror like characteristics and river marks in some regions. The addition of 1 wt.% of CNC did not qualitatively change the aspect of the fracture that was also brittle. However, the addition of 1.35 wt.% of BC resulted in a completely different topology. The image shows an arrangement of layers, which could be related to the growth of the BC as a network of fibrils that are added as new layers as the culture proceeds. Castro et al. [68], showed a similar layered topology for a nanocomposite made with PVA and obtained from a BC grown in the same strain that the one used in this work. On the other hand, the CNC remain randomly dispersed in the WBPU and the low concentration does not allow to observe their presence.

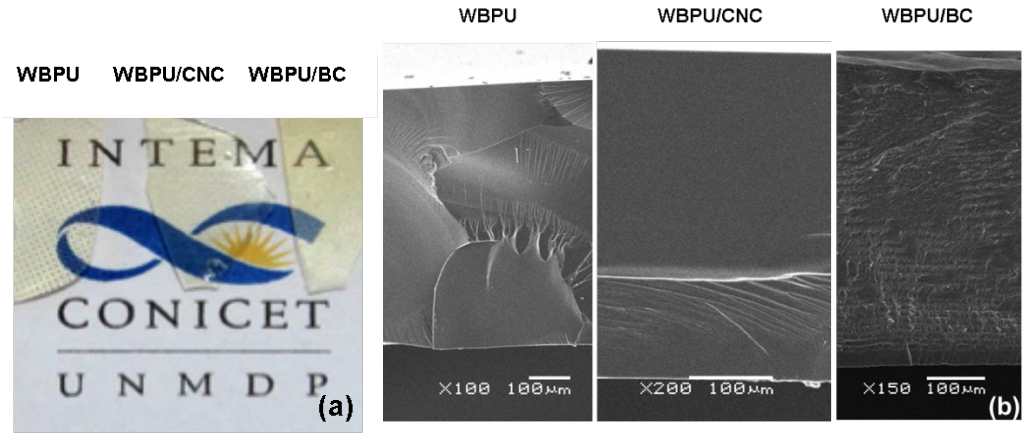

Figure 5. (a) Digital photography of the films; **(b)** SEM images of the fracture surface of the films. In both cases, the images correspond to: neat WBPU (left), WBPU/CNC (center) and WBPU/BC (right).

3.2.2. FTIR and DRX analysis of composites

Figure 6.a shows the FTIR spectra of the films. In the area of the bands located between 3500 cm^{-1} and 3100 cm^{-1} appear the characteristic peaks of cellulose and WBPU, overlapped in the composites and centered at 3335 cm^{-1}, corresponding to OH groups and mainly to the -N-H absorption in the PU [16]. It can also be observed that the intensity of this peak is slightly higher for the BC composite than that of the CNC composite, which may be attributed to the fact that in the latter, the surface OH groups have been partially replaced by sulfate groups [31,65,66].

The absorbance at 1710 cm^{-1} is attributed to hydrogen bonding of carbonyl stretching [69]; in the case of neat WBPU films this peak appears at 1702 cm^{-1} and is slightly shifted to 1697 cm^{-1} for the WBPU/CNC composite, which may be due to the hydrogen bonding interactions developed between the polymer and the reinforcement [15]. No shift is observed in the BC composite spectrum. On the other hand, it is observed that the peak at 1527 cm^{-1} shifts to a longer wavelength, 1537 cm^{-1} in the case of the CNC composite. This peak is attributed to N-H bending vibration of the urethane group of WBPU, thus the shift supports the already mentioned interactions between this reinforcement and the WBPU [70]. However, no shift is observed in the spectrum of the BC composite. Finally, in the case of composite with BC, the peaks marked with arrows in the zone between 1500-899 cm^{-1} correspond to absorption peaks of BC.

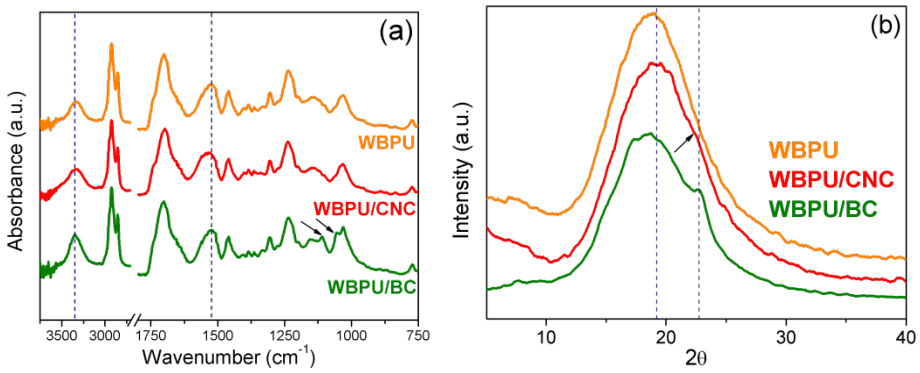

Figure 6. (a) FTIR spectra ; **(b)** X ray diffraction spectra of the neat WBPU and the nanocomposites.

Figure 6.b shows the X ray diffraction spectra of the neat polymer and nanocomposites. The amorphous nature of the WBPU results in the wide peak observed in the three spectra. However, the addition of BC can be confirmed by the presence of an overlapping small peak at ~22.6°, corresponding to the plane (110) of the BC. On the other hand, the addition of CNC only produces a very small shoulder in that same 2θ region (corresponding to the (002) plane of CNC). Additionally, a small shift of the amorphous peak towards higher angles can be detected. This change may be related to the good dispersion of the CNC and the interaction with the polymer structure.

3.2.3.Thermal characterization of the films (DSC, DMA and TGA)

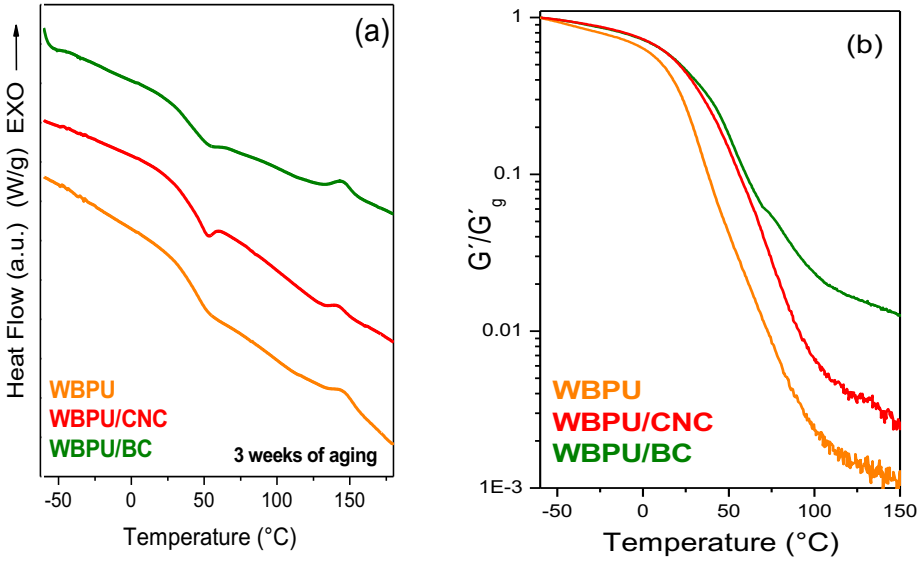

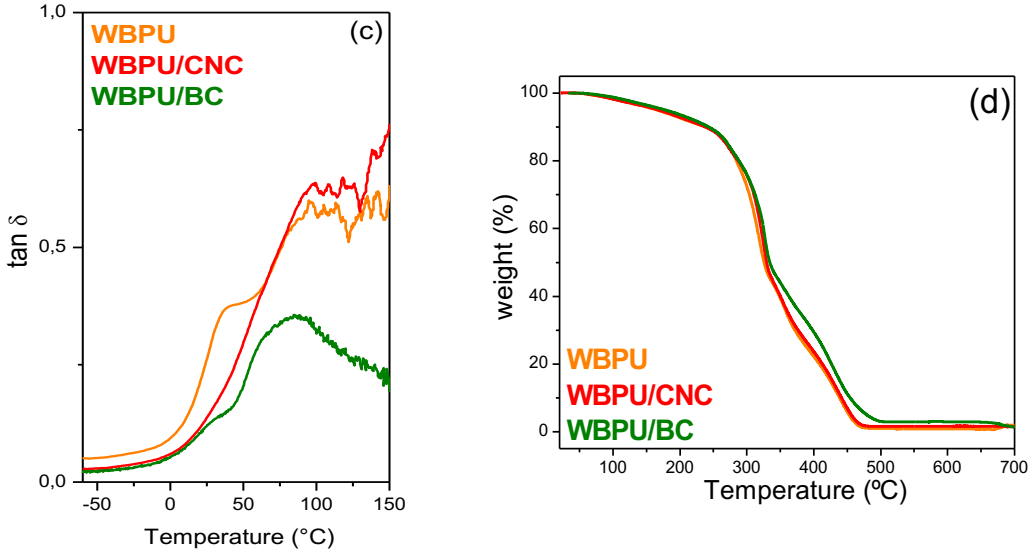

Figure 7. (a) DSC traces with 3 week of aging; **(b)** Normalized storage modulus; **(c)** tan δ of the films; **(d)** TG signal (residual weight %) of the films, neat WBPU and nanocomposites.

DSC characterization shows that a thermal event occurs at 56.4, 56.7 and 57.8 °C for WBPU, CNC composite and BC composite, respectively, which is associated to the glass transition temperature of the materials (Figure 7a). An endothermic peak associated to the event, which is due to densification of the PU during storage, appears in the DSC curves of the composites [71]. In those cases, to characterize the aged samples, the peak of the endotherm was considered as an estimation of the T_g reached in those conditions. Although after three weeks from preparation, densification has taken place in the composites, the endotherm is not present in the curve of the unreinforced WBPU. This suggests that the presence of the nanocelluloses accelerates the densification of the material.

Figure 7.a also shows an exothermal event occurring around 150 °C, which is associated to a transition of short range order-disorder corresponding to the hard segments of the WBPU (region associated to the reacted isocyanate molecules) [72–75].

The dynamic mechanical analysis (Figure 7.b) shows that the thermal transition from glass to rubber occurs in a wide temperature range, from about room temperature to above 100 °C. The curves of the normalized storage modulus (G'/G'_g) allow to clearly see the effect of the nanoparticles, producing a shift of the T_g of the somposites to higher temperatures. The tan δ plot (Figure 7.c) shows that the neat polymer has actually two relaxations, one close to room temperature and other one, more intense, around 90 °C. In the curves of the nanocomposites the low temperature relaxation is much reduced by the presence of the nanoparticles and relatively more in the case of the CNC films. On the other hand, the reduction of the main relaxation at higher temperature is more obvious in the case of the BC indicating that the mobility of all the polymer network structure has been reduced. Similar results have been reported by other authors for cellulose reinforced composite materials [76].

It is also interesting to compare the storage modulus of the different samples in the rubbery region. Clearly, the addition of the nanocelluloses results in the increase of the rubbery modulus, something to be expected because of the high modulus of the cellulose (~ 20-100 GPa, [20,77,78]) compared to that of the rubber modulus of the WBPU (G' at 100 °C was 1.3 MPa). The comparison also shows an additional interesting feature: the reinforcement of the BC is higher than that obtained with the CNC. For example, at 100 °C, the addition of the CNC resulted in a 4 times increase of the normalized modulus relative to neat WBPU, but more than 10 times in the BC case. This higher reinforcement is the

result of the 3D-cellulose network, that also led to the reduction of the tan δ peaks as it was already discussed.

Figure 7.d shows the thermal degradation traces of the neat polymer and the nanocomposites, where only the BC composite shows a small improvement in the thermal degradation. The temperature of the 5 % weight loss is shifted from 167 °C to 168 °C and 178 °C for WBPU/CNC and WBPU/BC, respectively. The same trend is observed in the temperature at which 90 % of the weight is lost, from 438 °C for the neat WBPU to 441 °C and 454 °C for the nanocomposites containing CNC and BC, respectively. All samples showed a very low residual char although slightly higher in the case of the composites compared to that of the neat WBPU. The improvement observed in the thermal stability for the bio-composites could be associated with the mechanical or chemical interaction between the bio-reinforcement and the matrix as it was reported by Amri et al. (2021) [79].

3.2.4. Static contact angle and water absorption

Figure 8 presents a summary of the results on static contact angle of water on the surface of the films. The upper surface of the films was used for the measurements. In all cases the angle was lower than 90° (hydrophilic surfaces), and particularly so in the case of the CNC nanocomposite and showing little change in the case of the WBPU/BC with respect to the unfilled polymer. Considering that nanocelluloses are hydrophilic and that BC has been identified as more hydrophilic than CNC [80], the explanation for these results could be find in the processing and distribution of the celluloses in the films. CNC are randomly distributed through the whole sample, since the distribution was obtained *via* mixing and ultrasonic stirring. Instead, the BC composite films were obtained by immersion/impregnation of the wet BC membrane. This last procedure is more prone to lead to the formation of a thin polymer region on the surfaces of the film than the procedure used with CNC. Figure 5.b also supports this view, since the layers of BC that can be seen in the internal part of the cross section of the film, are not present close to the surfaces Thus, CNC would be more exposed than the BC network and thus, surface hydrophobicity would be higher in WBPU/BC than in WBPU/CNC.

Additionally, the films were immersed in bi-distilled water for different lengths of time (Figure 8) and the result was the decohesion of the materials that broke into small pieces, with the exception of the BC nanocomposite. As it has been previously discussed, the BC forms a network of ribbons producing an interpenetrated network with the WBPU. The BC network is responsible for restricting the swelling and ultimately the fragmentation of the film.

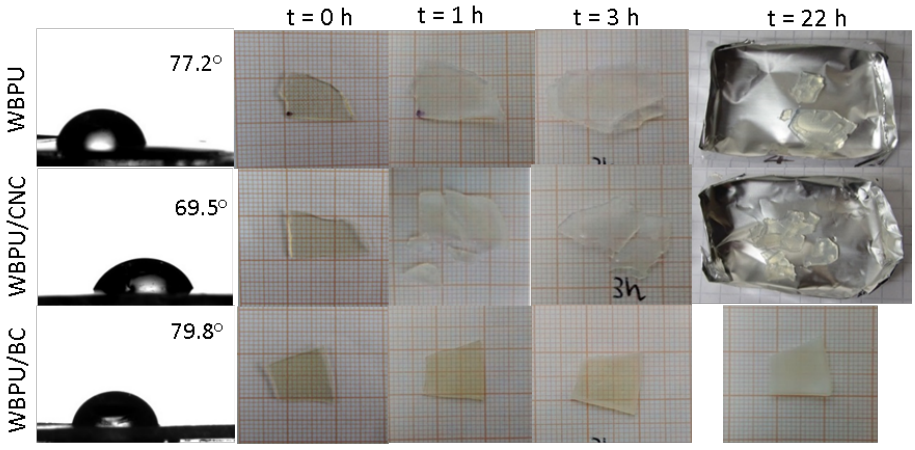

Figure 8. Behavior of the films in contact with water: contact angle and water immersion effect on the integrity of the films

4. Conclusions

Optically transparent bio-composite films from castor oil-based waterborne polyurethane (WBPU) reinforced with cellulose nanocrystal (CNC) and bacterial cellulose (BC) were obtained by means of two simple processing methodologies. The hydrophilic characteristics of both reinforcements favor its dispersion or impregnation with the WBPU aqueous dispersion.

The thermal stability of the BC was higher than that of the CNC, since the preparation method (acid hydrolysis) of the latter leaves sulfate groups on the surface and reduces its thermal stability. Despite this, both bio-reinforcement slightly increased the thermal stability of the bio-composites with respect to the polymeric matrix. This behavior would be associated with the mechanical and chemical interactions between polymer matrix and nanocellulose.

Compared to the matrix, the normalized storage modulus at the rubber state increased approximately 10 and 4 times for BC and CNC bio-composites, respectively. These results were a consequence of the interactions of the bio-reinforcement with the polymeric matrix. Particularly in the case of the BC based biocomposite, the results would be associated to the three-dimensional interconnected morphology of the bio-reinforcement. Even more interesting, the tridimensional structure of BC allowed to maintain the structural integrity of the composites films when being immersed in water.

Author Contributions: Conceptualization, V.M., P.S., M.I.A.; methodology, V.M. P.S., P.G.; validation, M.I.A., V.M..; formal analysis, M.E.V.H., M.I.A., V.M.; investigation, M.E.V.H., D.M.; data curation, M.E.V.H.; writing—original draft preparation, M.E.V.H.; writing—review and editing, M.I.A., V.M., P.S., M.E.V.H., P.G.; visualization, M.E.V.H.; supervision, M.I.A.; project administration, M.I.A.; funding acquisition, M.I.A., V.M. All authors have read and agreed to the published version of the manuscript.

Funding: We express our gratitude to the Consejo Nacional de Investigaciones Científicas y Técnicas (CONICET, Argentina) (PIP 2017 0100677), the Fondo para la Investigación Científica y Tecnológica (FONCYT) (PICT-2017- 1318), the Universidad Nacional de Mar del Plata (UNMdP, 15/G557, ING561/19) and to the Comisión de Investigaciones Científicas de la Provincia de Buenos Aires (CIC) and the Universidad Tecnológica Nacional (UTN) for their financial support.

Data Availability Statement: The data presented in this study are available on request from the corresponding author.

Acknowledgments: The authors also wish to thank to Dr. Cristina Castro Herazo for initial consultation on the BC culture and to Lic. Juan Buffa for obtaining the FE-SEM image of CNC.

Conflicts of Interest: The authors declare no conflict of interest. The funders had no role in the design of the study; in the collection, analyses, or interpretation of data; in the writing of the manuscript, or in the decision to publish the results.

References

1. Balart, R., Montanes, N., Dominici, F., Boronat, T. & Torres-Giner, S. Environmentally friendly polymers and polymer composites. *Materials.* **13,** 1–6 (2020).
2. Mishra, R. K., Ha, S. K., Verma, K. & Tiwari, S. K. Recent progress in selected bio-nanomaterials and their engineering applications: An overview. *J. Sci. Adv. Mater. Devices* **3,** 263–288 (2018).
3. Cao, X., Dong, H. & Li, C. M. New Nanocomposite Materials Reinforced with Flax Cellulose Nanocrystals in Waterborne Polyurethane. *Biomacromolecules* **8,** 899–904 (2007).
4. Madbouly, S. A., Xia, Y. & Kessler, M. R. Rheological behavior of environmentally friendly castor oil-based waterborne polyurethane dispersions. *Macromolecules* **46,** 4606–4616 (2013).
5. Saalah, S., Abdullah, L. C., Aung, M. M., Salleh, M. Z., Awang Biak, D. R., Basri, M., Jusoh, E. R. & Mamat, S. Colloidal stability and rheology of jatropha oil-based waterborne polyurethane (JPU) dispersion. *Prog. Org. Coatings* **125,** 348–357 (2018).
6. Mosiewicki, M. A. & Aranguren, M. I. Recent Developments in Plant Oil Based. *Polym. Int.* **65,** 28–38 (2016).

7. Liang, H., Liu, L., Lu, J., Chen, M. & Zhang, C. Castor oil-based cationic waterborne polyurethane dispersions: Storage stability, thermo-physical properties and antibacterial properties. *Ind. Crops Prod.* **117,** 169–178 (2018).
8. Moreno, M., Goikoetxea, M. & Barandiaran, M. J. Fatty Acid-Based Waterborne Coatings in *Biobased Environ. Benign Coatings* (eds. Tiwari, A., Galanis, A. & Soucek, M. D.) 161–182 (Scrivener Publishing LLC-Wiley, Beverly) (2016)
9. Madbouly, S. A. & Otaigbe, J. U. Recent advances in synthesis, characterization and rheological properties of polyurethanes and POSS/polyurethane nanocomposites dispersions and films. *Prog. Polym. Sci.* **34,** 1283–1332 (2009).
10. Xia, Y. & Larock, R. C. Preparation and properties of aqueous castor oil-based polyurethane-silica nanocomposite dispersions through a sol-gel process. *Macromol. Rapid Commun.* **32,** 1331–1337 (2011).
11. Choi, S. H., Kim, D. H., Raghu, A. V., Reddy, K. R., Lee, H. Il, Yoon, K. S., Jeong, H. M. & Kim, B. K. Properties of graphene/waterborne polyurethane nanocomposites cast from colloidal dispersion mixtures. *J. Macromol. Sci. Part B Phys.* **51,** 197–207 (2012).
12. Fu, C., Hu, X., Yang, Z., Shen, L. & Zheng, Z. Preparation and properties of waterborne bio-based polyurethane/siloxane cross-linked films by an in situ sol-gel process. *Prog. Org. Coatings* **84,** 18–27 (2015).
13. Liao, L., Li, X., Wang, Y., Fu, H. & Li, Y. Effects of surface structure and morphology of nanoclays on the properties of jatropha curcas oil-based waterborne polyurethane/ clay nanocomposites. *Ind. Eng. Chem. Res.* **55,** 11689–11699 (2016).
14. Gao, Z., Peng, J., Zhong, T., Sun, J., Wang, X. & Yue, C. Biocompatible elastomer of waterborne polyurethane based on castor oil and polyethylene glycol with cellulose nanocrystals. *Carbohydr. Polym.* **87,** 2068–2075 (2012).
15. Mondragon, G., Santamaria-Echart, A., Hormaiztegui, M. E. V., Arbelaiz, A., Peña-Rodriguez, C., Mucci, V., Corcuera, M., Aranguren, M. I. & Eceiza, A. Nanocomposites of Waterborne Polyurethane Reinforced with Cellulose Nanocrystals from Sisal Fibres. *J. Polym. Environ.* **26,** 1869–1880 (2018).
16. Hormaiztegui, M. E. V., Mucci, V. L. & Aranguren, M. I. Composite films obtained from a waterborne biopolyurethane. Incorporation of tartaric acid and nanocellulose. *Ind. Crops Prod.* **142,** 111879 (2019).
17. Cakić, S. M., Ristić, I. S., Stojiljković, D. T., Nikolić, N. N., Todorović, B. & Radosavljević-Stevanović, N. V. Effect of the silica nanofiller on the properties of castor oil-based waterborne polyurethane hybrid dispersions based on recycled PET waste. *Polym. Bull.* **76,** 1217–1238 (2019).
18. Fu, H., Wang, Y., Li, X. & Chen, W. Synthesis of vegetable oil-based waterborne polyurethane/silver-halloysite antibacterial nanocomposites. *Compos. Sci. Technol.* **126,** 86–93 (2016).
19. Panda, S. S., Panda, B. P., Mohanty, S. & Nayak, S. K. Synthesis and properties of castor oil-based waterborne polyurethane cloisite 30B nanocomposite coatings. *J. Coatings Technol. Res.* **14,** 377–394 (2017).
20. Eichhorn, S. J., Dufresne, A.., Aranguren, M., Marcovich, N. E., Capadona, J. R., Rowan, S. J., Weder, C., Thielemans, W., Roman, M., Renneckar, S., Gindl, W., Veigel, S., Keckes, J., Yano, H., Abe, K., Nogi, M., Nakagaito, A. N., Mangalam, A., Simonsen, J., Benight, A. S., Bismarck, A., Berglund, L. A. & Peijs, T. Review: Current international research into cellulose nanofibres and nanocomposites. *J. Mater. Sci.* **45,** (2010).
21. Miao, C. & Hamad, W. Y. Cellulose reinforced polymer composites and nanocomposites: A critical review. *Cellulose* **20,** 2221–2262 (2013).
22. Peng, B. L., Dhar, N., Liu, H. L. & Tam, K. C. Chemistry and applications of nanocrystalline cellulose and its derivatives: A nanotechnology perspective. *Can. J. Chem. Eng.* **89,** 1191–1206 (2011).
23. Buffa, J. M., Casado, U., Mucci, V. & Aranguren, M. I. Cellulose nanocrystals in aqueous suspensions: rheology of lyotropic chiral liquid crystals. *Cellulose* **26,** 2317–2332 (2019).
24. Casado, U., Mucci, V. L. & Aranguren, M. I. Cellulose nanocrystals suspensions: Liquid crystal anisotropy, rheology and films iridescence. *Carbohydr. Polym.* **261,** 117848 (2021).
25. Ludueña, L., Fasce, D., Alvarez, V. A. & Stefani, P. M. Nanocellulose from rice husk following alkaline treatment to remove silica. *BioResources* **6,** 1440–1453 (2011).
26. Qin, Y. Alginate fibers: an overwiew of the production processes and applications in wound management. *Polym. Int.* **57,** 171–180 (2008).
27. Auad, M. L., Richardson, T., Hicks, M., Mosiewicki, M. A., Aranguren, M. I. & Marcovich, N. E. Shape memory segmented polyurethanes: Dependence of behavior on nanocellulose addition and testing conditions. *Polym. Int.* **61,** 321–327 (2012).
28. Wang, J., Tavakoli, J. & Tang, Y. Bacterial cellulose production, properties and applications with different culture methods – A review. *Carbohydr. Polym.* **219,** 63–76 (2019).
29. Gallegos, A. M. A., Carrera, S. H., Parra, R., Keshavarz, T. & Iqbal, H. M. N. Bacterial cellulose: A sustainable source to develop value-added products - A review. *BioResources* **11,** 5641–5655 (2016).
30. Vasconcellos, V. M. & Farinas, C. S. The effect of the drying process on the properties of bacterial cellulose films from gluconacetobacter hansenii. *Chem. Eng. Trans.* **64,** 145–150 (2018).
31. Roman, M. & Winter, W. T. Effect of sulfate groups from sulfuric acid hydrolysis on the thermal degradation behavior of bacterial cellulose. *Biomacromolecules* **5,** 1671–1677 (2004).
32. Urbina, L., Alonso-Varona, A., Saralegi, A., Palomares, T., Eceiza, A., Corcuera, M. Á. & Retegi, A. Hybrid and biocompatible cellulose/polyurethane nanocomposites with water-activated shape memory properties. *Carbohydr. Polym.* **216,** 86–96 (2019).

33. Feng, Z., Li, M., Jin, X., Zheng, Y., Liu, J., Zhao, L., Wang, Y., Li, H. & Zuo, D. Design and characterization of plasticized bacterial cellulose/waterborne polyurethane composite with antibacterial function for nasal stenting. *Regen. Biomater.* **7,** 597–608 (2020).
34. Hormaiztegui, M. E. V., Daga, B., Aranguren, M. I. & Mucci, V. L. Bio-based waterborne polyurethanes reinforced with cellulose nanocrystals as coating films. *Prog. Org. Coatings* **144,** 105649 (2020).
35. Hormaiztegui, M. E. V., Aranguren, M. I. & Mucci, V. L. Synthesis and characterization of a waterborne polyurethane made from castor oil and tartaric acid. *Eur. Polym. J.* **102,** (2018).
36. Castro, C., Zuluaga, R., Putaux, J. L., Caro, G., Mondragon, I. & Gañán, P. Structural characterization of bacterial cellulose produced by Gluconacetobacter swingsii sp. from Colombian agroindustrial wastes. *Carbohydr. Polym.* **84,** 96–102 (2011).
37. Castro, C., Cleenwerck, I., Trcek, J., Zuluaga, R., de Vos, P., Caro, G., Aguirre, R., Putaux, J. L. & Gañán, P. Gluconacetobacter medellinensis sp. nov., cellulose- and non-cellulose-producing acetic acid bacteria isolated from vinegar. *Int. J. Syst. Evol. Microbiol.* **63,** 1119–1125 (2013).
38. Buffa, J. M., Grela, M. A., Aranguren, M. I. & Mucci, V. L. EPR spectroscopy applied to the study of the TEMPO mediated oxidation of nanocellulose. *Carbohydr. Polym.* **136,** 744–749 (2016).
39. Castro, C., Zuluaga, R., Álvarez, C., Putaux, J. L., Caro, G., Rojas, O. J., Mondragon, I. & Gañán, P. Bacterial cellulose produced by a new acid-resistant strain of Gluconacetobacter genus. *Carbohydr. Polym.* **89,** 1033–1037 (2012).
40. Yamanaka, S. & Sugiyama, J. Structural modification of bacterial cellulose. *Cellulose* **7,** 213–225 (2000).
41. Liang, C. Y. & Marchessault, R. H. Infrared spectra of crystalline polysaccharides. II. Native celluloses in the region from 640 to 1700 cm.1. *J. Polym. Sci.* **39,** 269–278 (1959).
42. Duchemin, B., Le Corre, D., Leray, N., Dufresne, A. & Staiger, M. P. All-cellulose composites based on microfibrillated cellulose and filter paper via a NaOH-urea solvent system. *Cellulose* 1–17 (2015).
43. Klemm, D., Philipp, B., Heinze, U. & Wagenknecht, W. in *Compr. Cellul. Chem. Fundam. Anal. Methods* **1,** 181–195 (1998).
44. Lu, J., Askeland, P. & Drzal, L. T. Surface modification of microfibrillated cellulose for epoxy composite applications. *Polymer (Guildf).* **49,** 1285–1296 (2008).
45. Kumar, A., Negi, Y. S., Choudhary, V. & Bhardwaj, N. K. Characterization of Cellulose Nanocrystals Produced by Acid-Hydrolysis from Sugarcane Bagasse as Agro-Waste. *J. Mater. Phys. Chem.* **2,** 1–8 (2014).
46. Borsoi, C., Zimmernnam, M. V. G., Zattera, A. J., Santana, R. M. C. & Ferreira, C. A. Thermal degradation behavior of cellulose nanofibers and nanowhiskers. *J. Therm. Anal. Calorim.* **126,** 1867–1878 (2016).
47. Morán, J. Extracción De Celulosa Y Obtención De Nanocelulosa a Partir De Fibra Sisal - Caracterización. *Genesis* 16–17 (2008).
48. Marcovich, N. E., Reboredo, M. M. & Aranguren, M. I. FTIR spectroscopy applied to woodflour. *Compos. Interfaces* **4,** 119–132 (1996).
49. Mosiewicki, M. A., Marcovich, N. E. & Aranguren, M. I. Characterization of fiber surface treatments in natural fiber composites by infrared and Raman spectroscopy. *Interface Eng. Nat. Fibre Compos. Maximum Perform.* 117–145 (2011).
50. Fan, M., Dai, D. & Huang, B. Fourier Transform Infrared Spectroscopy for Natural Fibres. *Fourier Transform - Mater. Anal.* 45–68 (2012).
51. Poletto, M., Pistor, V. & Zattera, A. J. Structural Characteristics and Thermal Properties of Native Cellulose in *Cellulose – Fundamental Aspects.*(eds. T. van de Ven, L. Godbout) 45–68 (IntechOpen, Rijeka) (2013).
52. Socrates, G. *Infrared and Raman Characteristic Group Frequencies*. Thir Edition (John Wiley & Sons Ltd., Middlesex) (2004)
53. Ciolacu, D., Ciolacu, F. & Popa, V. I. Amorphous Cellulose – Structure and Characterization. *Cellul. Chem. Technol.* **45,** 13–21 (2011).
54. Kafle, K., Greeson, K., Lee, C. & Kim, S. H. Cellulose polymorphs and physical properties of cotton fabrics processed with commercial textile mills for mercerization and liquid ammonia treatments. *Text. Res. J.* **84,** 1692–1699 (2014).
55. Lee, C. M., Mittal, A., Barnette, A. L., Kafle, K., Park, Y. B., Shin, H., Johnson, D. K., Park, S. & Kim, S. H. Cellulose polymorphism study with sum-frequency-generation (SFG) vibration spectroscopy: Identification of exocyclic CH2OH conformation and chain orientation. *Cellulose* **20,** 991–1000 (2013).
56. Elazzouzi-Hafraoui, S., Nishiyama, Y., Putaux, J. L., Heux, L., Dubreuil, F. & Rochas, C. The shape and size distribution of crystalline nanoparticles prepared by acid hydrolysis of native cellulose. *Biomacromolecules* **9,** 57–65 (2008).
57. Kulkarni, P. K., Anil Dixit, S. & Singh, U. B. Evaluation of bacterial cellulose produced form Acetobacter xylinum as pharmaceutical excipient. *Am. J. Drug Discov. Dev.* **2,** 72–86 (2012).
58. Vazquez, A., Foresti, M. L., Cerrutti, P. & Galvagno, M. Bacterial Cellulose from Simple and Low Cost Production Media by Gluconacetobacter xylinus. *J. Polym. Environ.* **21,** 545–554 (2013).
59. Park, S., Baker, J. O., Himmel, M. E., Parilla, P. a & Johnson, D. K. Cellulose crystallinity index: measurement techniques and their impact on interpreting cellulase performance. *Biotechnol. Biofuels* **3,** 10 (2010).
60. Garvey, C. J., Parker, I. H. & Simon, G. P. On the interpretation of X-ray diffraction powder patterns in terms of the nanostructure of cellulose I fibres. *Macromol. Chem. Phys.* **206,** 1568–1575 (2005).
61. Ahvenainen, P., Kontro, I. & Svedström, K. Comparison of sample crystallinity determination methods by X-ray diffraction for challenging cellulose I materials. *Cellulose* **23,** 1073–1086 (2016).
62. Jiang, F. & Hsieh, Y. Lo. Chemically and mechanically isolated nanocellulose and their self-assembled structures. *Carbohydr.*

Polym. **95,** 32–40 (2013).
63. Sofla, M. R. K., Brown, R. J., Tsuzuki, T. & Rainey, T. J. A comparison of cellulose nanocrystals and cellulose nanofibres extracted from bagasse using acid and ball milling methods. *Adv. Nat. Sci. Nanosci. Nanotechnol.* **7,** 035004 (2016).
64. Torgbo, S. & Sukyai, P. Biodegradation and thermal stability of bacterial cellulose as biomaterial: The relevance in biomedical applications. *Polym. Degrad. Stab.* **179,** 109232 (2020).
65. George, J., Sajeevkumar, V. A., Kumar, R., Ramana, K. V., Sabapathy, S. N. & Bawa, A. S. Enhancement of Thermal Stability Associated with the Chemical Treatment of Bacterial (Gluconacetobacter xylinus) Cellulose. *J. Appl. Polym. Sci.* **108,** 1845–1851 (2008).
66. Lichtenstein, K. & Lavoine, N. Toward a deeper understanding of the thermal degradation mechanism of nanocellulose. *Polym. Degrad. Stab.* **146,** 53–60 (2017).
67. Wang, N., Ding, E. & Cheng, R. Thermal degradation behaviors of spherical cellulose nanocrystals with sulfate groups. *Polymer (Guildf).* **48,** 3486–3493 (2007).
68. Castro, C., Vesterinen, A., Zuluaga, R., Caro, G., Filpponen, I., Rojas, O. J., Kortaberria, G. & Gañán, P. In situ production of nanocomposites of poly(vinyl alcohol) and cellulose nanofibrils from Gluconacetobacter bacteria: Effect of chemical crosslinking. *Cellulose* **21,** 1745–1756 (2014).
69. Lu, Y. & Larock, R. C. Soybean-oil-based waterborne polyurethane dispersions: Effects of polyol functionality and hard segment content on properties. *Biomacromolecules* **9,** 3332–3340 (2008).
70. Lei, L., Zhang, Y., Ou, C., Xia, Z. & Zhong, L. Synthesis and characterization of waterborne polyurethanes with alkoxy silane groups in the side chains for potential application in waterborne ink. *Prog. Org. Coatings* **92,** 85–94 (2016).
71. Pascault, J.-P., Sautereau, H., Verdu, J. & Williams, R. J. J. Thermosetting Polymers. First Edition(CRC Press, Ney York) (2002)
72. Hormaiztegui, M. E. V., Mucci, V. L., Santamaria-Echart, A., Corcuera, M. Á., Eceiza, A. & Aranguren, M. I. Waterborne polyurethane nanocomposites based on vegetable oil and microfibrillated cellulose. *J. Appl. Polym. Sci.* **133,** (2016).
73. Santamaria-Echart, A., Fernandes, I., Barreiro, F., Retegi, A., Arbelaiz, A., Corcuera, M. A. & Eceiza, A. Development of waterborne polyurethane-ureas added with plant extracts: Study of different incorporation routes and their influence on particle size, thermal, mechanical and antibacterial properties. *Prog. Org. Coatings* **117,** 76–90 (2018).
74. Jiang, L., Xu, Q. & Hu, C. P. Preparation and characterization of waterborne polyurethaneurea composed of dimer fatty acid polyester polyol. *J. Nanomater.* **2006,** 1–10 (2006).
75. Alonso-Lerma, B., Larraza, I., Barandiaran, L., Ugarte, L., Saralegi, A., Corcuera, M. A., Perez-Jimenez, R. & Eceiza, A. Enzymatically produced cellulose nanocrystals as reinforcement for waterborne polyurethane and its applications. *Carbohydr. Polym.* **254,** 117478 (2021).
76. Romanzini, D., Lavoratti, A., Ornaghi, H. L., Amico, S. C. & Zattera, A. J. Influence of fiber content on the mechanical and dynamic mechanical properties of glass/ramie polymer composites. *Mater. Des.* **47,** 9–15 (2013).
77. Vincent, J. F. V. From cellulose to cell. *J. Exp. Biol.* **202,** 3263–3268 (1999).
78. Mariano, M., Kissi, N. El & Dufresne, A. Cellulose Nanocrystals and Related Nanocomposites : Review of some Properties and Challenges. 791–806 (2014).
79. Amri, M. R., Guan, C. T., Osman Al-Edrus, S. S., Md Yasin, F. & Mohamad, S. F. Effect of Cellulose Nanofibrils on the Properties of Jatropha Oil-Based Waterborne Polyurethane Nanocomposite Film. *Polymers.* **13,** 1460 (2021).
80. Naomi, R., Idrus, R. B. H. & Fauzi, M. B. Plant-vs. Bacterial-derived cellulose for wound healing: A review. *Int. J. Environ. Res. Public Health* **17,** 1–25 (2020).